



# Synthesis, characterization, crystal structure and DFT studies on 3-(1H-benzo[d][1,2,3]triazol-1-yl)-1-oxo-1-*m*-tolylpropan-2-yl-nicotinate

Pusu Zhao<sup>a,\*</sup>, Xiumei Gao<sup>b</sup>, Jie Song<sup>a</sup>, Xiaojun Sun<sup>a</sup>, Wu lan Zeng<sup>c</sup>

<sup>a</sup> Jiangsu Key Laboratory for Chemistry of Low-Dimensional Materials, Huaiyin Normal University, Huaian, Jiangsu 223300, PR China

<sup>b</sup> Department of Computer Science and Technology, Huaiyin Normal University, Huaian, Jiangsu 223300, PR China

<sup>c</sup> MicroScale Science Institute, Department of Chemistry and Chemical Engineering, Weifang University, Weifang 261061, China

## ARTICLE INFO

### Article history:

Received 20 December 2010

Received in revised form 5 February 2011

Accepted 16 February 2011

### Keywords:

N-heterocyclic compound

Synthesis

Crystal structure

UV–vis spectrum

Fluorescence spectrum

DFT calculation

## ABSTRACT

3-(1H-Benzo[d][1,2,3]triazol-1-yl)-1-oxo-1-*m*-tolylpropan-2-yl-nicotinate (BOTN) has been synthesized and characterized by elemental analysis, IR, UV–vis and fluorescence spectroscopy. Its crystal structure has also been determined by X-ray single crystal diffraction. For BOTN, density functional theory (DFT) calculations of the structure and vibrational frequencies have been performed at B3LYP/6-311G\*\* level. The comparisons between the experimental vibrational frequencies and the predicted data show that B3LYP/6-311G\*\* method can simulate the IR of BOTN on the whole. Based on the vibration analysis, thermodynamic properties of BOTN have been calculated. The correlative equations between the thermodynamic properties and the temperatures have also been listed. The experimental UV–vis spectra present two peaks and theoretical UV–vis spectra obtained by TD-DFT method exhibit three peaks. The comparison between them suggests that the B3LYP/6-311G\*\* method can only approximately simulate the UV–vis spectra of BOTN. The fluorescence determination reveals two emission bands at 423 and 489 nm, respectively.

© 2011 Elsevier B.V. All rights reserved.

## 1. Introduction

As N-heterocyclic compounds, benzotriazole and its derivatives have attracted considerable attentions in industry and agriculture because of their significant biological activities including efficient antifungal, antitumor and antineoplastic activities [1–4]. Also, benzotriazoles are extensively used as synthetic auxiliaries in organic chemistry [5–7] and versatile ligands in coordination chemistry [8,9]. For example, the deprotonated benzotriazolate anion can coordinate up to three metal centres via its three nitrogen donors [10,11] and the copper complexes of benzotriazole drew many attentions due to the importance of benzotriazole as a corrosion inhibitor [12,13]. Recently, benzotriazoles have also been used as luminescent materials and fluorescent chemical sensor laser dyes [14,15]. However, to the best of our knowledge, among so many reported benzotriazoles, 1H-benzotriazole derivatives containing one nicotinato group are very rare. Herein, we report the four-steps synthesis and characterization on the title compound of 3-(1H-benzo[d][1,2,3]triazol-1-yl)-1-oxo-1-*m*-tolylpropan-2-yl-nicotinate (BOTN). The crystal structure, fluorescent spectra along with the density func-

tional theory (DFT) calculational results about BOTN are also reported.

## 2. Experimental and theoretical methods

### 2.1. Physical measurements

Elemental analyses for carbon, hydrogen and nitrogen were performed by a Perkin-Elmer 240C elemental instrument. The melting points were determined on a Yanaco MP-500 melting point apparatus. IR spectra (4000–400 cm<sup>-1</sup>), as KBr pellets, were recorded on a Nicolet FT-IR spectrophotometer. Electronic absorption spectra were measured on a Shimadzu UV3100 spectrophotometer in EtOH solution and solid state fluorescence spectra were measured on a F96-fluorescence spectrophotometer.

### 2.2. Synthesis of BOTN

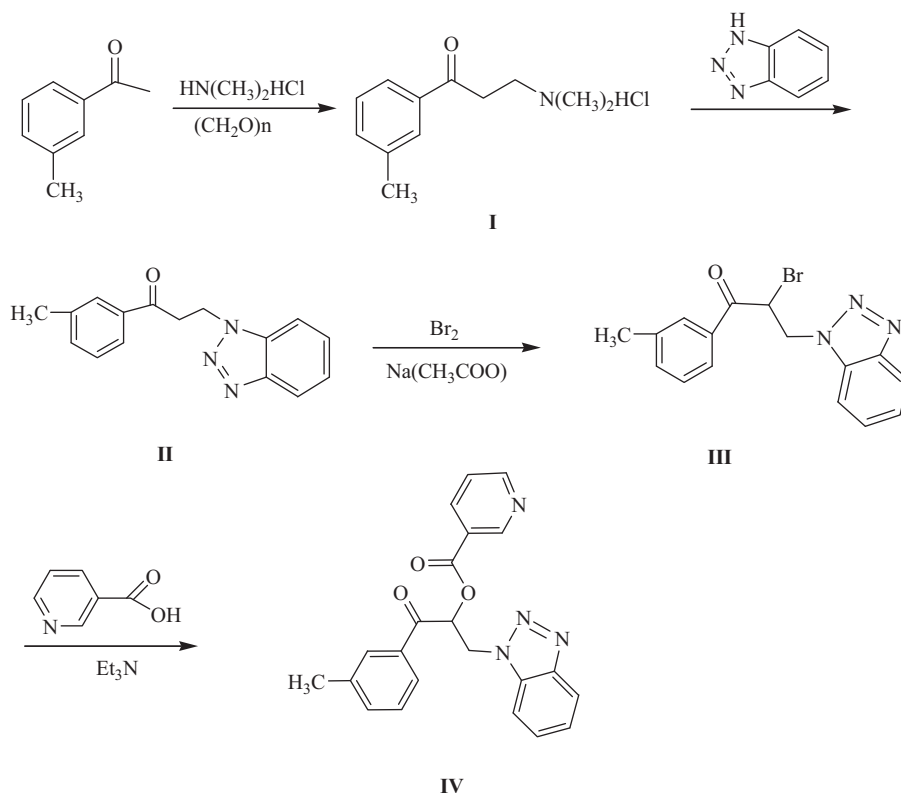
All chemicals were obtained from a commercial source and used without further purification.

The synthetic route is shown in Scheme 1.

Firstly, the intermediate **II** were prepared according to our earlier report [16]. IR  $\nu$  (KBr disc)/cm<sup>-1</sup>: 3092(m), 2921(m), 1624(s), 1584(s), 1486(m), 1472(m), 1375(m), 1361(m), 1268(s), 1213(m), 1060(m), 970(m), 914(m), 879(m), 850(m), 610(m). <sup>1</sup>H NMR (DMSO,  $\delta$ , ppm): 2.35(s, 3H, -CH<sub>3</sub>), 3.03(m, 2H -CH<sub>2</sub>), 3.92(m, 2H,

\* Corresponding author. Tel.: +86 0517 83525083; fax: +86 0517 83525085.

E-mail address: [zhaopusu@163.com](mailto:zhaopusu@163.com) (P. Zhao).



Scheme 1.

–CH<sub>2</sub>), 7.20–7.98(m, 8H, ArH). <sup>13</sup>C NMR (DMSO, δ, ppm): 24.1, 37.7, 43.5, 118.2, 125.8, 127.2, 128.4, 129.3, 133.2, 136.4, 138.2, 145.5, 200.3.

Secondly, the intermediate **II** (5.31 g, 0.02 mol) and sodium acetate (1.6 g, 0.02 mol) were dissolved in acetic acid (50 mL). Then, bromine (3.2 g, 0.02 mol) was added dropwise with stirring at 55–60 °C. After the mixture being stirring for 8 h, water (50 mL) and chloroform (20 mL) were added. The organic layer was washed successively with saturated sodium bicarbonate solution.

The washed solution was purified by flash column chromatography (silica gel, using V petroleum ether:V acetic ether = 4:1 as eluent) to afford intermediate **III**. IR ν (KBr disc)/cm<sup>-1</sup>: 3092(m), 3024(m), 2965(m), 2921(m), 1624(s), 1572(s), 1486(m), 1472(m), 1375(m), 1361(m), 1329(s), 1268(s), 1213(m), 1198(m), 1152(m), 971(m), 915(m), 879(m), 851(m), 610(m). <sup>1</sup>H NMR (DMSO, δ, ppm): 2.35(s, 3H, –CH<sub>3</sub>), 4.26(d, 2H –CH<sub>2</sub>), 4.92(m, 1H, –CH), 7.20–7.98(m, 8H, ArH). <sup>13</sup>C NMR (DMSO, δ, ppm): 24.1, 50.6, 57.6, 118.3, 125.8, 127.4, 128.4, 129.3, 32.9, 133.5, 136.4, 138.2, 145.5, 191.3

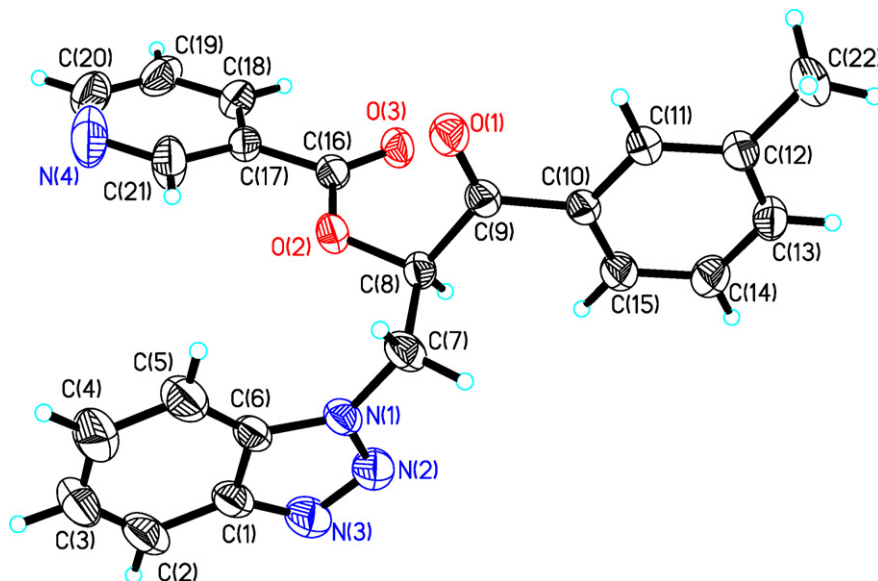


Fig. 1. The molecular structure with the atomic numbering for BOTN.

**Table 1**  
Summary of crystallographic results for BOTN.

Empirical formula	C <sub>22</sub> H <sub>18</sub> N <sub>4</sub> O <sub>3</sub>
Formula weight	386.40
Temperature, K	293(2)
Wavelength, Å	0.71073
Crystal system, space group	Monoclinic, P2(1)/c
Unit cell dimensions	
<i>a</i> (Å)	10.094(3)
<i>b</i> (Å)	9.331(3)
<i>c</i> (Å)	20.682(6)
β (°)	96.575(5)
Volume (Å <sup>3</sup> )	1935.2(10)
Z, calculated density (Mg m <sup>-3</sup> )	4, 1.326
Absorption coefficient (mm <sup>-1</sup> )	0.091
F(000)	808
θ range for data collection (°)	2.03–24.99
Limiting indices	−12 ≤ <i>h</i> ≤ 11, −11 ≤ <i>k</i> ≤ 10, −18 ≤ <i>l</i> ≤ 24
Reflections collected/unique	9829/3398 [ <i>R</i> <sub>int</sub> = 0.0529]
Refinement method	Full-matrix least-squares on <i>F</i> <sup>2</sup>
Data/restraints/parameters	3398/1/263
Goodness-of-fit on <i>F</i> <sup>2</sup>	1.085
Final <i>R</i> indices [ <i>I</i> > 2σ( <i>I</i> )]	<i>R</i> <sub>1</sub> = 0.0504, <i>wR</i> <sub>2</sub> = 0.1240
<i>R</i> indices (all data)	<i>R</i> <sub>1</sub> = 0.0901, <i>wR</i> <sub>2</sub> = 0.1472
Extinction coefficient	0.0066(15)
Largest diff. peak and hole	0.216 and −0.160 e Å <sup>-3</sup>

Thirdly, in a 100 mL flask, the intermediate **III** (5.16 g, 0.015 mol) was dissolved in acetone (20 mL), then nicotinic acid (2.46 g, 0.02 mol) and triethylamine (2.8 mL, 0.0175 mol) were added and the mixture was stirred at 0–5 °C. 5 h later, solid materials were observed and reaction was stopped. The mixtures were filtered and the filtrate was concentrated by rotary vacuum evaporation. Then, the concentrated filtrate was re-dissolved in chloroform (30 mL) and was washed three times with distilled water (30 mL) by using extraction method. Finally, the organic layer was rotary vacuum evaporation to obtain the **IV**. Yield 50.6%. m.p. 141.3–142.3 °C. Found: C, 68.13; H, 4.56; N, 14.34%. Calc. for C<sub>22</sub>H<sub>18</sub>N<sub>4</sub>O<sub>3</sub>: C, 68.38; H, 4.70; N, 14.50%. IR ν (KBr disc)/cm<sup>-1</sup>: 3068(m), 2980(m), 1720(s), 1690(s), 1590(s), 1567(m), 1499(m), 1466(m), 1388(m), 1337(s), 1254(s), 1224(s), 1088(m), 1050(w), 984(m), 950(w), 853(m), 773(m), 680(w), 620(w), 509(w). <sup>1</sup>H NMR (DMSO, δ, ppm): 2.35(s, 3H, −CH<sub>3</sub>), 4.31(s, 2H, −CH<sub>2</sub>), 5.54(s, 1H, −CH), 7.20–7.88(m, 8H, ArH, 1H in pyriding ring), 8.30(d, 1H in pyridyl ring), 8.89(d, 1H in pyridyl ring), 9.20(s, 1H in pyriding ring). <sup>13</sup>C NMR (DMSO, δ, ppm):

**Table 2**  
Selected geometric parameters by X-ray and theoretical calculations for BOTN at B3LYP/6-311G\*\* level.

Bond	Bond lengths (Å)		Bond	Bond lengths (Å)	
	Exp.	Calc.		Exp.	Calc.
O(1)–C(9)	1.214(3)	1.212	O(2)–C(16)	1.346(3)	1.358
O(3)–C(16)	1.202(2)	1.206	O(2)–C(8)	1.439(2)	1.431
N(1)–C(6)	1.352(3)	1.366	N(1)–N(2)	1.359(3)	1.366
N(1)–C(7)	1.454(3)	1.450	N(2)–N(3)	1.307(3)	1.287
N(3)–C(1)	1.366(3)	1.378	C(1)–C(6)	1.385(3)	1.408
C(2)–C(3)	1.345(5)	1.382	C(4)–C(5)	1.357(4)	1.384
C(7)–C(8)	1.519(3)	1.354	C(8)–C(9)	1.533(3)	1.545
C(10)–C(15)	1.394(3)	1.403	C(11)–C(12)	1.384(3)	1.394
N(4)–C(20)	1.343(5)	1.337	N(4)–C(21)	1.343(4)	1.334
C(17)–C(18)	1.366(3)	1.397	C(12)–C(22)	1.498(3)	1.510
Bond angle	Bond angle (°)		Bond angle	Bond angle (°)	
	Exp.	Calc.		Exp.	Calc.
C(16)–O(2)–C(8)	114.55(16)	115.92	N(1)–C(7)–C(8)	111.87(19)	112.51
C(10)–C(9)–C(8)	119.7(2)	118.35	O(3)–C(16)–O(2)	122.6(2)	123.09
O(2)–C(8)–C(9)	110.47(17)	110.28	N(3)–N(2)–N(1)	108.4(2)	109.49
C(6)–N(1)–N(2)	110.27(19)	109.97	C(2)–C(3)–C(4)	122.3(3)	121.33
C(20)–N(4)–C(21)	116.1(3)	117.37	C(18)–C(17)–C(21)	117.6(2)	118.36
C(11)–C(10)–C(15)	118.67(19)	119.34	C(13)–C(14)–C(15)	120.1(2)	120.32

**Table 3**  
Intermolecular hydrogen bonds and C–H...π supramolecular interactions.<sup>a</sup>

D–H...A	Symmetry	D...A (Å)	∠D–H...A (°)
C(7)–H(7A)...O(3)	1 – <i>x</i> , –1/2 + <i>y</i> , 1/2 – <i>z</i>	3.0317	112.64
C(21)–H(21A)...O(2)		2.7640	100.36
C(5)–H(5A)...Cg(4)	1 – <i>x</i> , –1/2 + <i>y</i> , 1/2 – <i>z</i>	3.939	160.92
C(18)–H(18A)...Cg(4)	1 – <i>x</i> , 1/2 + <i>y</i> , 1/2 – <i>z</i>	3.497	93.60
C(22)–H(22B)...Cg(1)	1 – <i>x</i> , –1/2 + <i>y</i> , 1/2 – <i>z</i>	3.924	122.22

<sup>a</sup> C(1) ring denotes triazolyl ring N(1)–N(2)–N(3)–C(1)–C(6); C(4) ring denotes phenyl ring C(10)–C(15).

**Table 4**  
π...π stacking interactions.<sup>a</sup>

Cg(I)...Cg(J)	Symmetry	Distance between ring centroids (Å)	Perpendicular distance of Cg(I) on ring J (Å)	Perpendicular distance of Cg(J) on ring I (Å)
Cg(1)...Cg(3)	1 – <i>x</i> , – <i>y</i> , 1 – <i>z</i>	3.768	3.608	3.610
Cg(3)...Cg(1)	1 – <i>x</i> , – <i>y</i> , 1 – <i>z</i>	3.768	3.610	3.608

<sup>a</sup> C(1) ring denotes triazolyl ring N(1)–N(2)–N(3)–C(1)–C(6); C(3) ring denotes phenyl ring C(1)–C(6).

24.1, 53.2, 84.0, 118.2, 122.0, 125.8, 127.2, 128.0, 129.3, 133.2, 136.4, 138.2, 145.5, 151.1, 166.1, 197.0.

Single crystal of BOTN suitable for X-ray measurements was obtained by recrystallization from ethanol at room temperature.

### 2.3. Crystal structure determination

The selected colorless crystal of BOTN was mounted on a CCD area diffractometer. Reflection data were measured at 293.2 K using graphite monochromated Mo-Kα (λ = 0.71073 Å) radiation and a φ-ω scan mode. The structure was solved by direct methods and refined by full-matrix least-squares method on *F*<sub>obs</sub><sup>2</sup> using the SHELXTL software package [17]. All non-H atoms were anisotropically refined. The hydrogen atom positions were fixed geometrically at calculated distances and allowed to ride on the parent C atoms. The final least-square cycle gave *R* = 0.0504, *wR*<sub>2</sub> = 0.1240 for 2064 reflections with *I* > 2σ(*I*) using the weighting scheme, *w* = 1/[σ<sup>2</sup>(*F*<sub>o</sub><sup>2</sup>) + (0.0618*P*)<sup>2</sup>], where *P* = (*F*<sub>o</sub><sup>2</sup> + *F*<sub>c</sub><sup>2</sup>)/3. Atomic scattering factors and anomalous dispersion corrections

**Table 5**  
Comparison of the observed and calculated vibrational spectra of BOTN.<sup>a</sup>

Assignments	Exp.	B3LYP/6-311G**
Phenyl ring and pyridyl ring C–H str.	3068	3110–3024
–CH <sub>3</sub> and –CH <sub>2</sub> C–H str.	2980	3009–2908
C=O str.	1720	1719
C=O str.	1690	1693
Phenyl ring and pyridyl ring C–C str. + C–N str.	1590, 1567	1591–1547
Phenyl ring and pyridyl ring C–H ip. def.	1499, 1466	1466–1448
–CH <sub>3</sub> C–H rock		1428
–CH <sub>2</sub> C–H rock		1417
Phenyl ring and pyridyl ring C–H ip. def.	1388	1398–1379
–CH and –CH <sub>2</sub> C–H rock	1337	1346–1337
Phenyl ring and pyridyl ring C–H ip. def.	1254	1306–1259
C–O str.	1224	1224
Phenyl ring and pyridyl ring C–H ip. def.	1088	1090–1080
C(8)–C(9) str.	1050	1041
N–N str.	984	984
Phenyl ring and pyridyl ring C–H opp. def.	950	979–955
Phenyl ring and pyridyl ring C–H opp. def.	853	894
Phenyl ring and pyridyl ring C–H opp. def.	773	791–752
Phenyl ring and pyridyl ring C–H opp. def.	680	700–663
Phenyl ring and pyridyl ring C–C def. + C–N def.	620	625–607
Whole molecular skeleton def.	509	509

<sup>a</sup> The atomic numbering scheme is as shown in Fig. 1. str.: stretch; ip: in-plane; oop: out-of-plane; def.: deformation.

were taken from International Table for X-ray Crystallography [18]. The key crystallographic data are given in Table 1.

#### 2.4. Computational methods

Initial molecular geometry was optimized using MM + molecular modeling and semi-empirical AM1 methods [19] (HYPERCHEM 6.0, Hypercube, Ont., Canada). Then, DFT calculations with a hybrid functional B3LYP at basis set 6-311G\*\* by the Bery method [20] were performed with the Gaussian 03 software package [21]. The calculated vibrational frequencies ascertained that the structure was stable (no imaginary frequencies). Based on the optimized geometry and by using time-dependent density functional theory (TD-DFT) [22–24] methods, electronic spectra of the title compound were predicted.

All calculations were performed on a DELL PE 2850 server and a Pentium IV computer using the default convergence criteria

**Table 6**  
Thermodynamic properties at different temperatures at B3LYP/6-311G\*\* level.

T (K)	C <sub>p,m</sub> <sup>0</sup> (J mol <sup>-1</sup> K <sup>-1</sup> )	S <sub>m</sub> <sup>0</sup> (J mol <sup>-1</sup> K <sup>-1</sup> )	H <sub>m</sub> <sup>0</sup> (kJ mol <sup>-1</sup> )
200.0	285.24	637.57	34.56
298.1	409.79	774.46	68.62
300.0	412.15	777.00	69.38
400.0	533.05	912.51	116.78
500.0	634.14	1042.71	175.32
600.0	714.86	1165.75	242.92
700.0	779.20	1280.96	317.74
800.0	831.17	1388.51	398.35

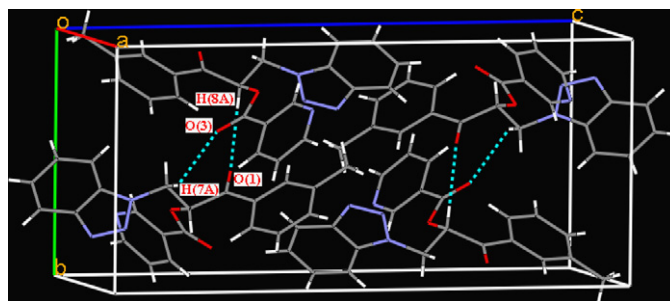


**Fig. 2.** Packing diagram of the unit cell along the *a*-axis for BOTN. The distances of C(7)–H(7A)···O(3) and C(21)–H(21A)···O(2) are 3.0317 and 2.7640 Å, respectively.

### 3. Results and discussion

#### 3.1. Description for the crystal structure of BOTN

For BOTN, the displacement ellipsoid plot with the numbering scheme is shown in Fig. 1. Fig. 2 shows a perspective view of the crystal packing in the unit cell. Selected bond lengths and bond angles by X-ray diffractions are listed in Table 2 along with the calculated bond parameters.

The molecular structure of BOTN consists of discrete [CH<sub>3</sub>PhCOCHCH<sub>2</sub>C<sub>5</sub>H<sub>4</sub>NCOOPhN<sub>3</sub>] entities. All of the bond lengths and bond angles in the phenyl ring, pyridyl ring and benzotriazole ring are in the normal range. All of the C–O bond lengths are also in the normal range. The phenyl ring along with the methyl group and atoms C(9) and O(1) define a plane *P1*, with the biggest deviation being 0.046 Å for C(9) atom. The pyridyl ring along with the atom C(16) define another plane *P2*, with the biggest deviation being –0.015 Å for C(18) atom. The benzotriazole ring and the joined atom of C(7) are also coplanar to *P3*, with the biggest deviation being 0.007 Å for C(7) atom. The dihedral angles between the *P1*–*P2*, *P1*–*P3* and *P2*–*P3* are 82.34(2), 16.20(3) and 83.00(3)°, respectively.

In the crystal lattice, there are three potentially weak intermolecular interactions (C–H···Y, Y=O) [25,26], three C–H···π supramolecular interactions and two π···π stacking interactions (see Tables 3 and 4), which make BOTN to be three-dimension (3D) network and stabilize the crystal structure.

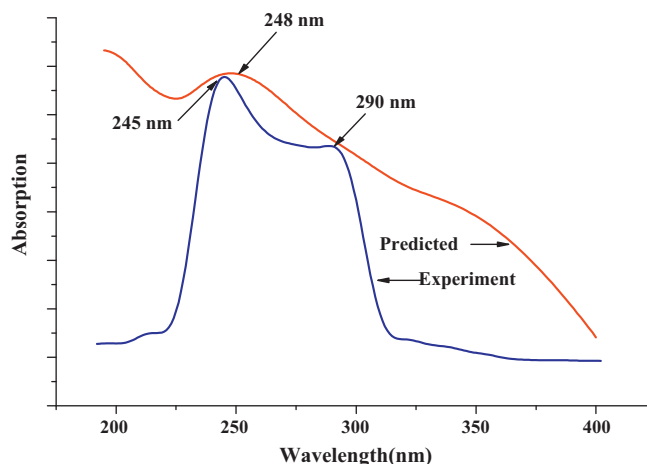


**Fig. 3.** Experimental and theoretical electronic spectra for BOTN.

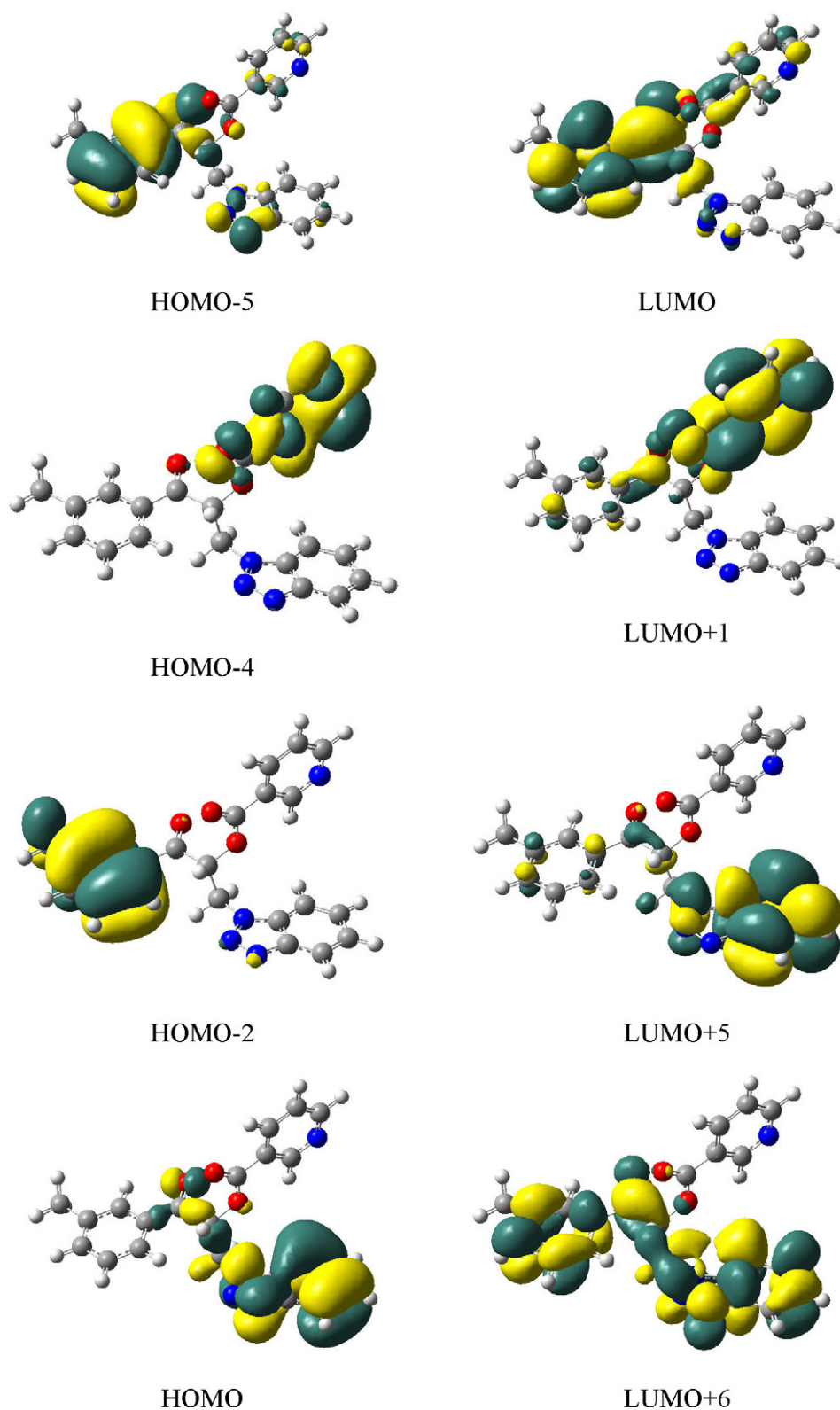


Fig. 4. Isodensity surfaces of eight frontier molecular orbitals for BOTN.

### 3.2. Optimized geometry

The optimized geometry of BOTN has been obtained at B3LYP/6-311G\*\* level. To make the comparison easy, the calculated geometric parameters of the title compound are also included in Table 2.

As seen in Table 2, most of the predicted geometric parameters have higher values than those determined experimentally. Comparing the predicted values with the experimental ones, it can be found that the biggest difference in bond angles occurs at the C(16)–O(2)–C(8) bond angle with the difference being 1.37°. Considering the bond lengths, the biggest variation between the

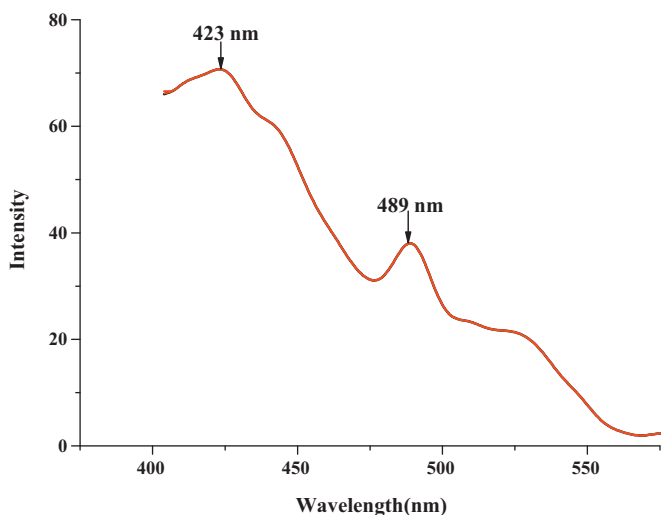
**Table 7**  
Experimental and theoretical UV–vis spectra values.

Exp.			Calc. (TD-DFT)	
Wave length (nm)	log $\epsilon$	Wave length (nm)	Oscillator strength	Electronic transition modes
245	1.95	200	0.2945	101 (HOMO) → 107 (LUMO + 5) 101 (HOMO) → 108 (LUMO + 6) 96 (HOMO-5) → 102 (LUMO)
290	1.55	248	0.1099	96 (HOMO-2) → 103 (LUMO + 1) 97 (HOMO-4) → 102 (LUMO)
		331	0.0045	101 (HOMO) → 102 (LUMO)

experimental and predicted values can be found at bond C(7)–C(8), with the difference being 0.165 Å. This is most likely due to the fact that the experimental data describe BOTN in the solid state, whereas the calculated data correspond to the molecule in the gas phase. The geometry of the solid-state structure is subject to intermolecular forces, such as van der Waals interactions, crystal packing forces, hydrogen-bond forces and the other types of supramolecular interactions. For example, the bonds of C(7)–H(7A) and C(8)–H(8A) and the atom O(2) all involve in forming hydrogen bonds, which make the experimental geometric parameters around the above three atoms have bigger differences from the calculated ones. In spite of these differences, the predicted molecular structure can simulate the crystal structure on the whole. Based on the optimized structure, thermodynamic properties and the UV spectra of BOTN are obtained.

### 3.3. Vibrational frequency

Vibrational frequencies of BOTN have been calculated and scaled by 0.96 [27], which is a typical scaled factor for the calculated method. Some primary calculated harmonic frequencies are listed in Table 5 and compared with the experimental data. The descriptions concerning the assignment have also been indicated in Table 5. Gauss-view program [28] has been used to assign the calculated harmonic frequencies. Seen from Table 5, by using the B3LYP/6-311G\*\* method, all of the experimental vibrational bands can be predicted and the predicted vibrational frequencies are in good agreement with experimental values except that two C–H stretch vibrations frequencies of 1428 and 1417  $\text{cm}^{-1}$  for methyl group and methylene group, which can not be found in experiment. Namely, on the whole, the B3LYP/6-311G\*\* method can be used to predict the vibrational frequencies.

**Fig. 5.** Solid-state fluorescence spectra of BOTN.

### 3.4. Thermodynamic properties

For BOTN, on the basis of vibrational analyses and statistical thermodynamics, the standard thermodynamic functions: heat capacity ( $C_{p,m}^0$ ), entropy ( $S_m^0$ ) and enthalpy ( $H_m^0$ ) were obtained and listed in Table 6. The scale factor for frequencies is also 0.96 [27].

As observed in Table 6, with the temperature increasing from 200.0 to 800.0 K, all the values of  $C_{p,m}^0$ ,  $S_m^0$  and  $H_m^0$  increase, which is attributed to the enhancement of the molecular vibration while the temperature increases.

The correlation equations between these thermodynamic properties and temperature  $T$  are as follows:

$$C_{p,m}^0 = -33.647 + 1.746 T - 8.315 \times 10^{-4} T^2 \quad (R^2 = 0.9998)$$

$$S_m^0 = 332.502 + 1.583 T - 3.277 \times 10^{-4} T^2 \quad (R^2 = 0.99998)$$

$$H_m^0 = -17.181 + 0.156 T + 4.572 \times 10^{-4} T^2 \quad (R^2 = 0.9998)$$

These equations will be useful for the further studies on BOTN.

### 3.5. UV–vis absorption spectra

For BOTN, UV–vis absorption spectra have been measured in EtOH solution at room temperature. To compare the experimentally obtained spectra with theoretical values, TD-DFT method has been applied to predict UV–vis spectra based on the B3LYP/6-311G\*\* level optimized structure. Both the experimental and predicted UV–vis spectra are shown in Fig. 3. The theoretical UV–vis spectra are drawn using the SWizard program, revision 4.5 [29,30]. The detailed experimental and theoretical UV–vis spectra values are listed in Table 7. Seen from Fig. 3, in experiment, there exist two peaks at 245 and 290 nm, respectively. In theory, there are three peaks is at 200, 248 and 331 nm. Therefore, for the system studied here, TD-DFT-B3LYP/6-311G\*\* level can approximately simulate the experimental electronic spectra. Fig. 4 shows the isodensity surfaces of eight frontier molecular orbitals for BOTN, which all are corresponding with the electronic transitions listed in Table 7. As seen from Fig. 4, in eight frontier molecular orbitals, the electron clouds are mainly distributed on phenyl ring, pyridyl ring, benzotriazole ring and three oxygen atoms, respectively, which suggest that the electronic transitions in UV–vis spectra are corresponding to the  $n \rightarrow \pi^*$  and  $\pi \rightarrow \pi^*$  electron transitions. For example, the electron transitions related with the transition peak at 331 nm are mainly assigned to two electronic transition modes, HOMO-4 → LUMO and HOMO → LUMO. In HOMO-4 and HOMO, electron clouds are mainly distributed on pyridyl ring, benzotriazole ring and oxygen atoms, while in LUMO, the electron clouds are mainly distributed on phenyl ring along with oxygen atoms. Then, the electron transitions related with the transition peak at 331 nm are mainly from pyridyl ring, benzotriazole ring and oxygen atoms to phenyl ring and oxygen atoms, which are corresponding to the  $n \rightarrow \pi^*$  and  $\pi \rightarrow \pi^*$  electron transitions.

### 3.6. Fluorescence spectra

Experimental solid-state fluorescence spectra of BOTN are shown in Fig. 5. The emission bands are observed at 423 and 489 nm, respectively, which lie in the blue region, indicating that BOTN is a potential fluorescent material.

### 4. Conclusions

3-(1H-Benzo[d][1,2,3]triazol-1-yl)-1-oxo-1-*m*-tolylpropan-2-yl-nicotinate (BOTN) has been synthesized by four-step reactions and characterized by IR and UV–vis spectra. The crystal structure determinations show that the compound crystallizes in monoclinic, space group  $P2(1)/c$ . B3LYP/6-311G\*\* method can simulate the crystal structure and vibrational spectra of BOTN on the whole. Based on the calculational vibration frequencies, the thermodynamic properties of BOTN have been obtained. The TD-DFT method at B3LYP/6-311G\*\* level can be used to predict the electronic spectra approximately. The solid-fluorescence spectra determinations suggest that BOTN is a potential fluorescent material.

### Acknowledgements

This work was supported by Jiangsu Key Laboratory for Chemistry of Low-Dimensional Materials, PR China (JSKC10078) and Huaian Science & Technology Bureau, Jiangsu Province, PR China (HAG2010027).

### Appendix A. Supplementary data

Supplementary data associated with this article can be found, in the online version, at doi:10.1016/j.saa.2011.02.040.

### References

- [1] K.Z. Katarzyna, N. Andzelika, Z. Justyna, C. Lidia, P. Janusz, M. Przemysław, B. Maria, *Bioorg. Med. Chem.* 12 (2004) 2617–2624.
- [2] M.D. Kamal, A.G. Hassan, E. Mohey, A.M. Hanan, H. Bahira, *Bioorg. Med. Chem.* 14 (2006) 3672–3680.
- [3] C.Y. Wu, K.Y. King, C.J. Kuo, J.M. Fang, Y.T. Wu, M.Y. Ho, C.L. Liao, J.J. Shie, P.H. Liang, C.H. Wong, *Chem. Biol.* 13 (2006) 261–268.
- [4] S.S. Zhang, H.Q. Zhang, D. Li, L.H. Sun, C.P. Ma, W. Wang, J. Wan, B. Qu, *Eur. J. Pharmacol.* 584 (2008) 144–152.
- [5] A.R. Katritzky, R.M. Witek, V. Rodriguez-Garcia, P.P. Mohapatra, J.W. Rogers, J. Cusido, A.A.A. Abdel-Fattah, P.J. Steel, *J. Org. Chem.* 70 (2005) 7866–7881.
- [6] Y.H. Kang, C.J. Lee, K. Kim, *J. Org. Chem.* 66 (2001) 2149–2153.
- [7] A.R. Katritzky, D.N. Haase, J.V. Johnson, A. Chung, *J. Org. Chem.* 74 (2009) 2028–2032.
- [8] C. Richardson, P.J. Steel, *Dalton Trans.* (2003) 992–1000.
- [9] X.L. Zhou, X.R. Meng, W. Cheng, H.W. Hou, M.S. Tang, Y.T. Fan, *Inorg. Chim. Acta* 360 (2007) 3467–3474.
- [10] D.S. Moore, S.D. Robinson, *Adv. Inorg. Chem.* 32 (1988) 171–239, and references therein.
- [11] M. Murrie, D. Collison, C.D. Garner, M. Helliwell, P.A. Tasker, S.S. Turner, *Polyhedron* 17 (1998) 3031–3043.
- [12] D.A. Pillard, J.S. Cornell, D.L. Dufresne, M.T. Hernandez, *Water Res.* 35 (2001) 557–560.
- [13] K.F. Khaled, *Electrochim. Acta* 54 (2009) 4345–4352.
- [14] M.C. Hu, Y. Wang, Q.G. Zhai, S.N. Li, Y.C. Jiang, Y. Zhang, *Inorg. Chem.* 48 (2009) 1449–1468.
- [15] T.Z. Yu, Y.L. Zhao, X.S. Ding, D.W. Fang, L. Aian, W.K. Dong, *J. Photochem. Photobiol. A* 188 (2007) 245–251.
- [16] W.L. Zeng, *Acta Crystallogr. E* 63 (2007) o3219–o3220.
- [17] G.M. Sheldrick, *SHELXTL, v5 Reference Manual*, Siemens Analytical X-Ray Systems, Madison, WI, 1997.
- [18] A.J. Wilson, *International Table for X-ray Crystallography*, Kluwer Academic, Dordrecht, The Netherlands, 1992, Vol. C: Tables 6.1.1.4 (pp. 500–502) and 4.2.6.8 (pp. 219–222).
- [19] M.J.S. Dewar, E.G. Zoebisch, E.F. Healy, *J. Am. Chem. Soc.* 107 (1985) 3902–3909.
- [20] C. Peng, P.Y. Ayala, H.B. Schlegel, M.J. Frisch, *J. Comput. Chem.* 17 (1996) 49–56.
- [21] M.J. Frisch, G.W. Trucks, H.B. Schlegel, G.E. Scuseria, M.A. Robb, J.R. Cheeseman, J.A. Montgomery, Jr., K.N. Kudin, J.C. Burant, J.M. Millam, S.S. Iyengar, J. Tomasi, V. Barone, B. Mennucci, M. Cossi, G. Scalmani, N. Rega, G.A. Petersson, H. Nakatsuji, M. Hada, M. Ehara, K. Toyota, R. Fukuda, J. Hasegawa, M. Ishida, T. Nakajima, Y. Honda, O. Kitao, H. Nakai, M. Klene, X. Li, J.E. Knox, H.P. Hratchian, J.B. Cross, C. Adamo, J. Jaramillo, R. Gomperts, R.E. Stratmann, O. Yazyev, A.J. Austin, R. Cammi, C. Pomelli, J.W. Ochterski, P.Y. Ayala, K. Morokuma, G.A. Voth, P. Salvador, J.J. Dannenberg, V.G. Zakrzewski, S. Dapprich, A.D. Daniels, M.C. Strain, O. Farkas, D.K. Malick, A.D. Rabuck, K. Raghavachari, J.B. Foresman, J.V. Ortiz, Q. Cui, A.G. Baboul, S. Clifford, J. Cioslowski, B.B. Stefanov, G. Liu, A. Liashenko, P. Piskorz, I. Komaromi, R.L. Martin, D.J. Fox, T. Keith, M.A. Al-Laham, C.Y. Peng, A. Nanayakkara, M. Challacombe, P.M.W. Gill, B. Johnson, W. Chen, M.W. Wong, C. Gonzalez, J.A. Pople, *Gaussian Inc.*, Wallingford, CT, 2004.
- [22] E. Runge, E.K.U. Gross, *Phys. Rev. Lett.* 52 (1984) 997–1000.
- [23] M. Petersilka, U.J. Gossmann, E.K.U. Gross, *Phys. Rev. Lett.* 76 (1996) 1212–1215.
- [24] R. Bauernschmitt, R. Ahlrichs, *Chem. Phys. Lett.* 256 (1996) 454–464.
- [25] T. Steiner, *Cryst. Rev.* 6 (1996) 1–5.
- [26] G.A. Jeffrey, H. Maluszynska, J. Mitra, *Int. J. Biol. Macromol.* 7 (1985) 336–348.
- [27] J.A. Pople, H.B. Schlegel, R. Krishnan, D.J. Defrees, J.S. Binkley, M.J. Frisch, R.A. Whiteside, R.F. Hout, W.J. Hehre, *Int. J. Quantum Chem. Quantum Chem. Symp.* 15 (1981) 269–278.
- [28] A. Frish, A.B. Nielsen, A.J. Holder, *Gaussview Users Manual*, Gaussian Inc., Pittsburgh, 2000.
- [29] S.I. Gorelsky, *SWizard program*, <http://www.sg-chem.net/>, University of Ottawa, Ottawa, Canada, 2009.
- [30] S.I. Gorelsky, A.B.P. Lever, *J. Organomet. Chem.* 635 (2001) 187–196.